Supplementary Information (SI) for

Revealing the intrinsic nature of Cu- and Ce-doped Mn_3O_4 catalyst with positive and negative effects on CO oxidation using *operando* DRIFTS-MS

Zihao Hu[a], Xiaoying Zhou[b], Tiantian Zhang[ab] Zuliang Wu[b,c], Jing Li[b,c], Wei Wang[b,c], Erhao Gao[b,c], Jiali Zhu[b,c], Shuiliang Yao[a,b,c,*]

a. School of Environmental and Safety Engineering, Changzhou University, Changzhou, China
b. School of Environmental Science and Engineering, Changzhou University, Changzhou, China
c. Advanced Plasma Catalysis Engineering Laboratory for China Petrochemical Industry, Changzhou, China

*Corresponding author.
Email address: yaos@cczu.edu.cn (Shuiliang Yao)

1. Experimental section

1.1. Catalyst characterization

All prepared catalysts were characterized using scanning electron microscope (SEM), high resolution transmission electron microscope (HRTEM), automatic specific surface area and porosity analyzer (BET), X-ray diffractometer (XRD), X-ray photoelectron spectroscopy (XPS), Raman spectroscopy (Raman), and H_2 temperature-programmed reduction (H_2-TPR).

The SEM (ZEISS GeminiSEM 300, Germany) was used to observe the morphology of the sample. An appropriate amount of sample was directly adhered to the conductive adhesive, and then the sample morphology was photographed. The acceleration voltage was 3 kV when the morphology was photographed. The HRTEM (FEI Tecnai F20, USA) were used to measure the morphologies of the catalysts and the distribution of elements on the catalyst surfaces. The catalyst samples were prepared using a copper mesh, observed in high vacuum conditions at 200 kV. The specific surface and porosity analyzer (Micromeritics ASAP 2460, USA) was used for the determination of physical properties such as pore size, pore volume and specific surface area (based on Brunauer–Emmett–Teller (BET) method) of the catalysts. The catalyst sample to be tested was pretreated by degassing at 300 °C for 8 h. The XRD spectroscopy measurements were carried out using the X-ray diffractometer (Bruker D2 Phaser, Germany) with Cu Kα radiation source operated at current 40 mA and voltage 40 kV, angle range 10° to 80° with an angle step of 0.02° (minimum step size 0.0001°). The elemental distribution and valence states of the catalyst were determined using Thermo Scientific K-Alpha (Thermo Scientific, USA) with Al-Kα X-ray radiation (hv=1486.6 eV) as the excitation source. The Raman spectroscopy (Thermo Scientific DXR, USA) was used to measure the molecular vibration and rotation information of the material, and then the chemical bond and molecular structure of the material are analyzed. The test laser wavelength is 633, and the test range was 100 – 900 cm^{-1}. The H_2 temperature-programmed reduction (H_2-TPD) was carried out on Micromeritics AutoChem II 2920. The 50-80 mg samples were placed in a U-shaped quartz tube and dried at 10 °C/min from room temperature to 300 °C. He gas flow (50 mL min^{-1}) was purged for 1h and cooled to 50 °C. After the baseline was stabilized by 10%H_2/Ar gas mixture (50 mL min^{-1}) for 0.5 h, the sample was desorbed at 800 °C at a heating rate of 10 °C/min in 10% H_2/Ar gas flow, and the reducing gas was detected by TCD.

1.2. Experimental procedures of DRIFTS-MS analysis

All DRIFTS and MS spectra were collected after pretreatment under conditions listed in Table S1.

Supplementary Table S1. Conditions for DFIFTS-MS experiments.

Experiment	Condition
Pretreatment	The catalyst (around 100 mg, 40-60 mech) was fed with a 20 mL min^{-1} gas mixture of 10%O_2 with Ar balance at 300 °C for 30 min, then cooled to 25 °C.
CO oxidation in O_2/Ar	The catalyst was fed with a 25 mL min^{-1} gas mixture of 1%CO, 10%O_2, and Ar (balance) at 25 °C for 20 min, and heated to 400 °C with a ramp of 10 °C min^{-1}.
CO oxidation in Ar	The catalyst was fed with a 25 mL min^{-1} gas mixture of 1%CO balanced with Ar at 25 °C for 20 min, and heated to 400 °C with a ramp of 10 °C min^{-1}.

1.3. Calculations

The CO conversion x was calculated with Eq. S1:

$$x = \frac{[CO]_0 - [CO]}{[CO]_0} \times 100\% \quad \text{(S1)}$$

where, $[CO]_0$ and $[CO]$ are the CO concentrations in inlet and outlet gases from the reactor, respectively.

The conversion frequency *TOF* value in μmol $(g\ s)^{-1}$ was calculated using Eq. S2:

$$TOF = \frac{F \cdot [CO]_0 \cdot x}{m} \times 100\% \quad \text{(S2)}$$

where, F and m are the gas flow rate to the reactor in $m^3\ s^{-1}$ and catalyst weight in g, respectively.

The CO oxidation reaction on the catalyst obeys zero order reaction (Eq. S3) based on the experimental results. The rate constant k ($mol \cdot s^{-1}$) was calculated using Eq. S4. The apparent activation energy (E_a) was obtained using the Arrhenius relation (Eq. S5).

$$\frac{d[CO]}{dt} = -k \quad \text{(S3)}$$

$$k = \frac{F\,[CO]_0}{V_R} x \quad \text{(S4)}$$

$$lnk = -\frac{E_a}{RT} + lnA \quad \text{(S5)}$$

where V_R in m^3 is the volume of the catalyst layer in the reactor. R represents the gas constant in

J·(mol·K)$^{-1}$. T denotes CO oxidation reaction temperature in K. A is pre-exponential factor.

Grain size D of each catalyst was calculated using Sherrer's Eq. 6:

$$D = \frac{\alpha \lambda}{\beta cos\theta} \tag{S6}$$

where α is the Scherrer constant, λ is the X-ray wavelength, which is 1.54056 Å, β is the half-height width of the diffraction peak of the measured sample, and θ is the Bragg angle.

2. Figures

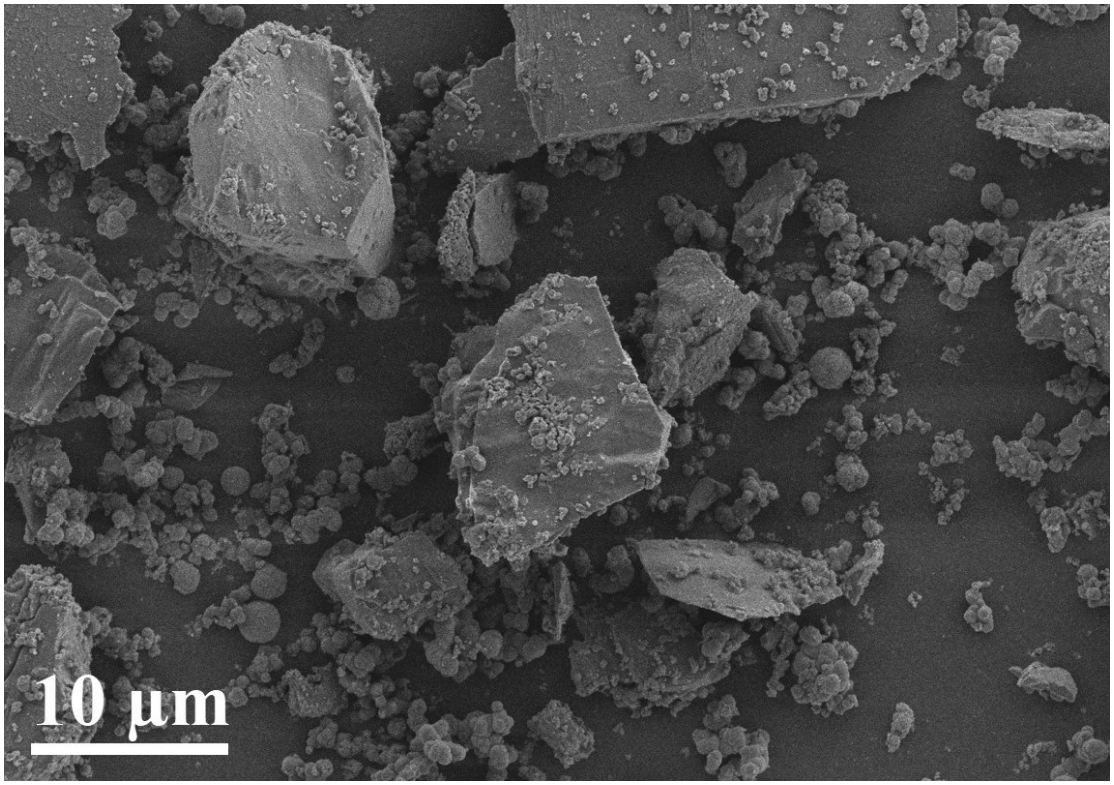

Fig. S1. SEM images of Mn-MOF-74.

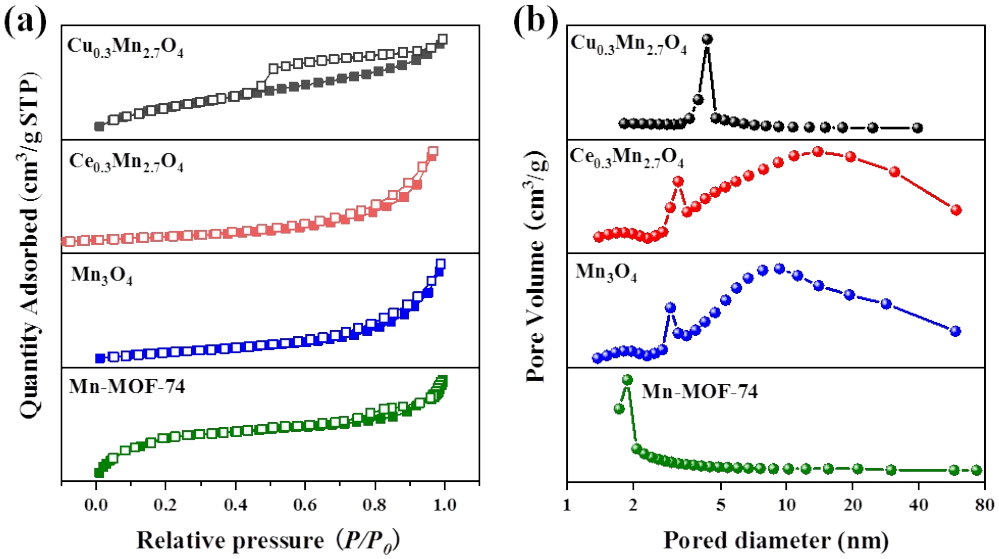

Fig. S2. (a) N_2 adsorption/desorption isotherm diagrams of $Cu_{0.3}Mn_{2.7}O_4$, $Ce_{0.3}Mn_{2.7}O_4$, and Mn_3O_4, (b) corresponding BJH pore size distribution diagrams.

Supplementary Table S2. Specific surface areas, pore volumes, pore sizes, T_{50}, T_{90}, and E_a of $Cu_{0.3}Mn_{2.7}O_4$, $Ce_{0.3}Mn_{2.7}O_4$, and Mn_3O_4 catalysts

Catalyst	BET Surface Area (m^2 g^{-1})	Pore Volume (cm^3 g^{-1})	Pore Size (nm)	T_{50} (°C)	T_{90} (°C)	E_a (kJ mol^{-1})	D (Å)
$Cu_{0.3}Mn_{2.7}O_4$	222.0	0.208	3.7	91	118	16.0	373
$Ce_{0.3}Mn_{2.7}O_4$	88.3	0.275	13.2	165	200	30.7	407
Mn_3O_4	96.3	0.278	11.9	148	190	27.73	982
Mn-MOF-74	452.2	0.351	3.18	/	/	/	/

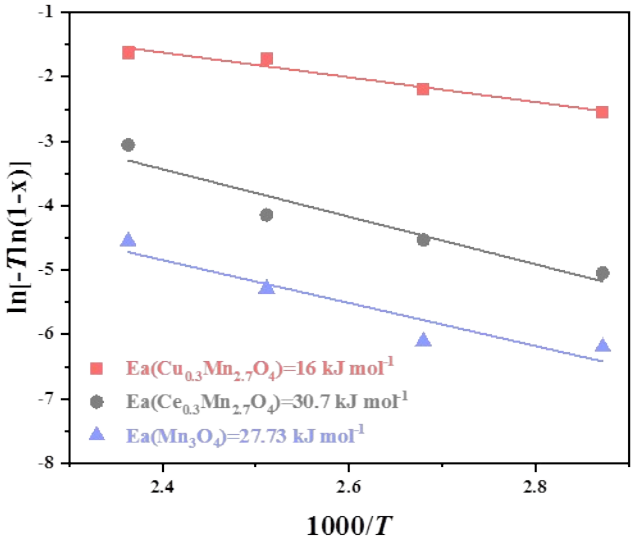

Fig. S3. E_a values of $Cu_{0.3}Mn_{2.7}O_4$, $Ce_{0.3}Mn_{2.7}O_4$, and Mn_3O_4.

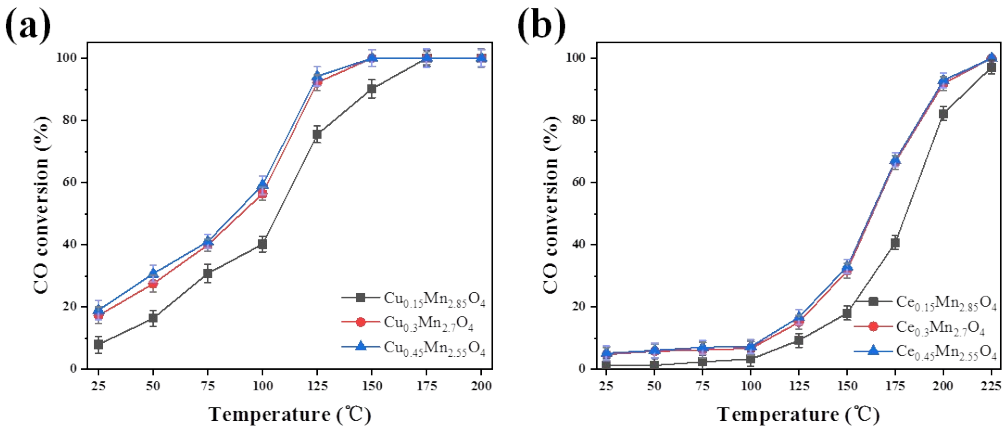

Fig. S4. (a) CO oxidation on $Cu_{0.15}Mn_{2.85}O_4$, $Cu_{0.3}Mn_{2.7}O_4$, and $Cu_{0.45}Mn_{2.55}O_4$ catalysts. (b) CO oxidation on $Ce_{0.15}Mn_{2.85}O_4$, $Ce_{0.3}Mn_{2.7}O_4$, and $Ce_{0.45}Mn_{2.55}O_4$ catalysts.

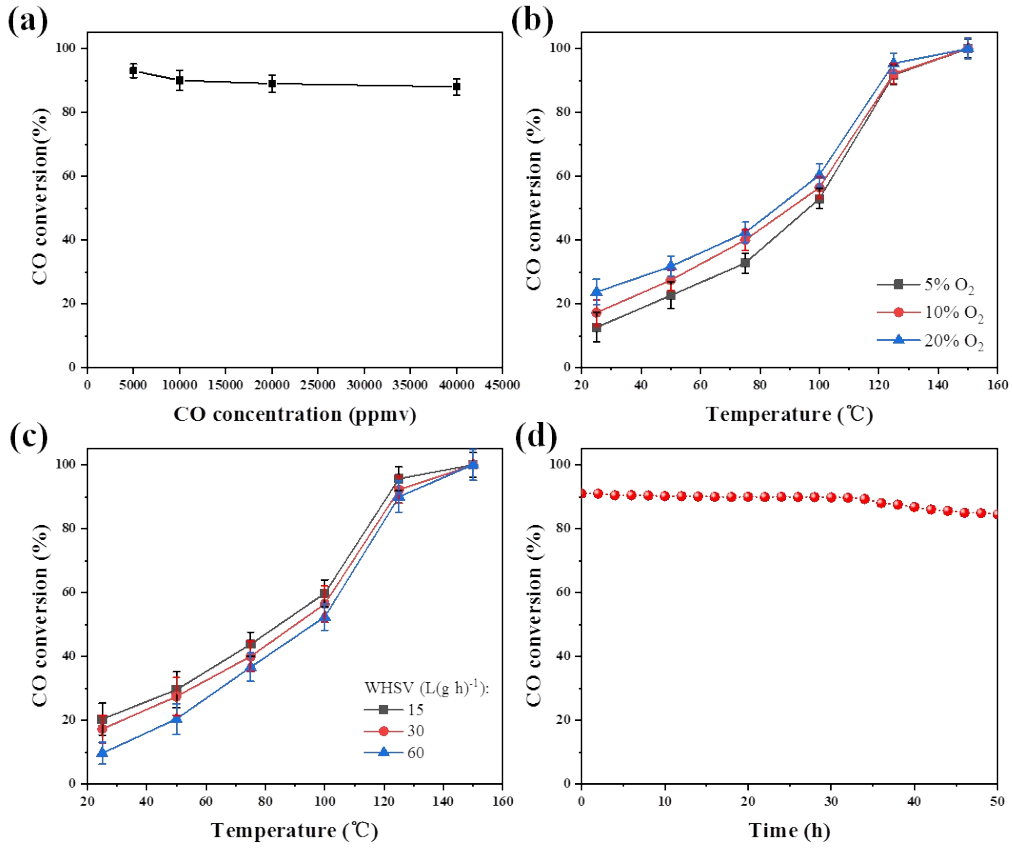

Fig. S5. Influence of various parameters on CO oxidation over $Cu_{0.3}Mn_{2.7}O_4$ catalyst. (a) The effect of initial CO concentration at a *WHSV* of 30 $L \cdot g^{-1} \cdot h^{-1}$, 10% O_2, and a temperature of 118 °C. (b) Temperature-dependent CO conversion at a *WHSV* of 30 $L \cdot g^{-1} \cdot h^{-1}$, 1% CO, and varying O_2 concentrations of 5%, 10%, or 20%. (c) CO conversion as a function of temperature at different *WHSV*s of 15, 30, or 60 $L \cdot g^{-1} \cdot h^{-1}$, with 1% CO and a constant 10% O_2. (d) Long-term stability test of CO oxidation at a temperature of 118 °C.

Supplementary Table S3. The experimental conditions and activities of various oxide catalysts for CO oxidation.

Catalyst	Preparation method	BET ($m^2\ g^{-1}$)	Experimental condition	Activity	References
Au/NiO	Deposition-precipitation	around 130	1% CO in air, 20 L h^{-1} g^{-1}	T_{50} = 65 °C, T_{90} = 150 °C	[1]
Ni-CeO_2	Synchronous spray-pyrolysis	110	1.0% CO, 1.0% O_2/He, 13.2 L h^{-1} g^{-1}	T_{50} = 100 °C, T_{90} = 140 ℃	[2]
$Ni_{1-x}Li_xO$	Sol-gel	9	1% CO, 22% O_2/N_2, 18 L g^{-1} h^{-1}	T_{50} = 140 °C, T_{90} = 240 ℃	[3]
Mn_3O_4/TiO_2	urea-assisted deposition	111	1% CO, 20.8% O_2/N_2, 30 L h^{-1} g^{-1}	T_{50} = 125 °C, T_{90} = 160 °C	[4]

Mn_3O_4/CeO_2	hydrothermal	99	1% CO/20% O_2/N_2, 60 L h^{-1} g^{-1}	T_{50} = 381 °C, T_{90}= 478 °C	[5]
$Cu_{0.3}Mn_{2.7}O_4$	hydrothermal	222	1%CO, 10% O_2/N_2, 30 L h^{-1} g^{-1}	T_{90}= 91 °C T_{90}= 118 °C	This study

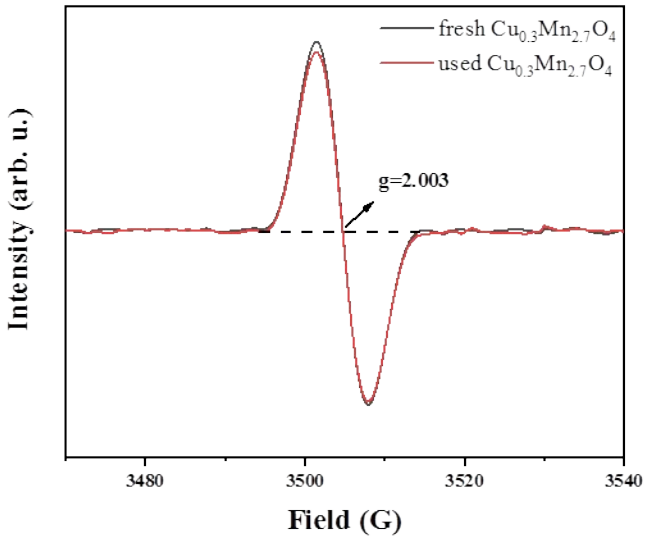

Fig. S6. EPR spectra for the $Cu_{0.3}Mn_{2.7}O_4$ catalyst before and after the stability test.

[1] Mochizuki C., Inomata Y., Yasumura S., et al. Defective NiO as a stabilizer for Au single-atom catalysts[J]. ACS Catalysis, 2022, 12(10): 6149-6158.

[2] Sun N., Xiang L., Zhuge B., et al. Atomically Incorporating Ni into Mesoporous CeO_2 Matrix via Synchronous Spray-Pyrolysis as Efficient Noble-Metal-Free Catalyst for Low-Temperature CO Oxidation[J]. Inorganic Chemistry, 2022, 62(2): 782-791.

[3] Xu X., Li L., Huang J., et al. Engineering Ni^{3+} cations in NiO lattice at the atomic level by Li^+ doping: the roles of Ni^{3+} and oxygen species for CO oxidation[J]. ACS Catalysis, 2018, 8(9): 8033-8045.

[4] Yi Y., Zhang P., Qin Z., et al. Low temperature CO oxidation catalysed by flower-like Ni–Co–O: how physicochemical properties influence catalytic performance[J]. RSC advances, 2018, 8(13): 7110-7122.

[5] Shu M., Wei S., Jia C.-J., et al. Effect of nickel oxide doping to ceria-supported gold catalyst for CO oxidation and water-gas shift reactions[J]. Catalysts, 2018, 8(12): 584.